Chapter 3

MEF2 activates DMPK expression promoting cardiomyocyte elongation and sarcomere degeneration

Ralph J. van Oort, Meriem Bourajjaj, Joost Schimmel, Melany C. van Oostrom, Roel van der Nagel, Igor I. Rybkin, Rhonda Bassel-Duby, Eric N. Olson, Elisabeth Ehler, Leon J. De Windt

Submitted

ABSTRACT

The heart responds to stress signals by hypertrophic growth, which is accompanied by activation of select transcription factors and reprogramming of cardiac gene expression. Although the transcription factor myocyte enhancer factor-2 (MEF2) is known to be a common endpoint for several hypertrophic pathways, its precise gene targets and role in myocardial remodeling remain to be elucidated. To this end, we pursued comprehensive gain-of-function approaches to activate MEF2 transcriptional activity in cultured cardiomyocytes. Adenoviral delivery of wildtype MEF2A or constitutively active MEF2 to cultured ventricular myocytes primarily induced myocyte elongation and myofibril degeneration, instead of concentric hypertrophy and sarcomere assembly, which one would expect for a hypertrophic effector.

To facilitate the identification of early MEF2 target genes underlying this cellular remodeling process, we combined an inducible gene expression system in a cardiac cell line with genome wide gene chip analyses, and found 75 MEF2 target genes at 24 hrs after inducible MEF2 activation. Gene ontology classification revealed an overrepresentation of genes involved in energy metabolism, cytoskeletal remodeling, and cell-matrix adhesion. Confocal analyses indicated that MEF2-induced myocyte elongation was accompanied by a redistribution of focal adhesions. SiRNA mediated knockdown of the MEF2 target gene myotonic dystrophy protein kinase (DMPK) was sufficient to inhibit MEF2 induced cardiomyocyte elongation.

Thus, these findings assign a novel function to MEF2 transcription factors in postnatal heart muscle, where they activate a gene program that promotes myocyte elongation, myofibril degeneration, and focal adhesion distribution in a DMPK-dependent fashion.

INTRODUCTION

The myocyte enhancer factor-2 (MEF2) transcription factor was originally defined as a muscle-specific DNA binding activity that recognizes conserved A/T-rich elements associated with numerous muscle-specific genes [1]. To date, four MEF2 genes, *mef2a*, *-b*, *-c*, and *-d*, have been characterized in vertebrates, with an expression pattern and function that extends beyond striated muscle. MEF2 transcription factors share high homology in an amino-terminal MADS (MCM1, Agamous, Deficiens, and Serum response factor) box and an adjacent MEF2-specific domain, which together mediate dimerization and binding to the consensus

DNA sequence CTA(A/T)$_4$TA(G/A) [2, 3]. MEF2 factors have been implicated in the embryonic development of cardiac, skeletal, and smooth muscle [4], and in postnatal heart disease [5, 6].

Soon after birth, cardiomyocytes withdraw from the cell cycle and heart growth occurs only by an increase in size of the individual myocytes. While this is a part of normal development and initially beneficial it can run out of control and the response to stress signals can lead to pathological hypertrophy and activation of a "fetal" cardiac gene program. Clinical stress signals that induce cardiac hypertrophy include hypertension, endocrine disorders, myocardial infarction, and contractile dysfunction from inherited mutations in cardiac structural genes. Pathological hypertrophy frequently progresses to dilated cardiomyopathy (DCM), a chronic disorder of the heart muscle. In humans, end-stage DCM is characterized by poorly contractile and dilated ventricles, accompanied by lengthening of myocytes, myocyte side-to-side slippage, loss of myofibrils, severe changes in cytoskeletal architecture and accumulation of collagen in perivascular and interstitial spaces [7, 8]. The genetic underpinnings underlying the cellular alterations in DCM remain largely elusive.

Thus far, MEF2 transcription factors have been postulated to play a role in the development of cardiac hypertrophy. In line with this premise, in normal adult myocardium, MEF2 exhibits only basal activity, likely required for the maintenance of contractile protein gene expression and energy metabolism [9, 10]. In cardiac disease, however, circumstantial evidence suggests that MEF2 factors serve as a transcriptional platform for prohypertrophic signaling cascades, including calcineurin, calcium/calmodulin-dependent protein kinase (CaMK), big mitogen-activated protein kinase (MAPK)-1 (BMK-1), and p38 MAPK [6, 11, 12].

In contrast, we and others have recently demonstrated that overexpression of MEF2 in the postnatal heart minimally triggers the hypertrophic growth response, but induces dilated cardiomyopathy [6, 13].

To further investigate the role of MEF2 in cardiomyocyte remodeling, we generated adenoviruses expressing either wildtype MEF2A or a constitutively active mutant of MEF2. Cultured ventricular myocytes infected with these viruses primarily underwent myocyte elongation, accompanied by sequential loss of myofibrils. A genome-wide gene chip analysis of early MEF2 target genes in a ventricular muscle cell line with inducible MEF2 activation provided mechanistic insights into the diverse cardiomyopathic consequences associated with MEF2 activation. Functional clustering of MEF2 target genes revealed an overrepresentation of genes involved in cytoskeletal remodeling and cell-matrix adhesion. In line, MEF2-induced myocyte elongation was accompanied by focal adhesion redistribution. One of the genes found to be upregulated by MEF2 activation was myotonic dystrophy protein kinase (DMPK). Inhibition of the MEF2

induced increase of DMPK protein levels resulted in partial rescue of the elongated phenotype, suggesting a primary role for DMPK in myocyte elongation and the genesis of dilated cardiomyopathy.

Table 1. List of oligonucleotide primers used for RT-PCR.

Gene	Accession number	Forward	Reverse
Acta1	NM_009606	5'-GCATGCAGAAGGAGATCACA	5'-ACATCTGCTGGAAGGTGGAC
CTGF	NM_010217	5'-AGACATACAGGGCTAAGTTCTG	5'-CACTGGCAGAGTGGTGGTTCT
DMPK	S60315	5'-GGACAAGTATGTGGCCGACT	5'-CATCTTCACCACCGCTACCT
Gsta1	NM_008181	5'-CGCCACCAAATATGACCTCT	5'-CAAGGCAGTCTTGGCTTCTC
Itga7	NM_008398	5'-AACAGCACCTTTCTGGAGGA	5'-GGATGCATCTCTGAGCAACA
Itgb4	BC059192	5'-CCTTCGAGCAGCCTGAATAC	5'-CTCCCTCCACAGGGACATAA
L7	BC086786	5'-GAAGCTCATCTATGAGAAGGC	5'-AAGACGAAGGAGCTGCAGAAC
Muc5b	NM_028801	5'-CTCTTCAACTCACGCATGGA	5'-TACACAGGCCTGACAGTTGC
Myl9	BC055439	5'-CAGAACCGAGATGGCTTCAT	5'-CCCCAAACATTGTGAGGAAC
Nexn	NM_199465	5'-AGAGGAAGAACGCAGGCATA	5'-GCTTGAATTGAGCCACTCCT
Sgca	NM_009161	5'-AGGCCCAGCAGACAACTTTA	5'-GGTGAGCGTGGTAGGTGAGT
Sgcb	NM_011890	5'-TGCTGAGGTTCAAGCAAGTG	5'-CTGGAAGACAATTGGCTGGT

MATERIALS AND METHODS

Recombinant adenoviruses. MEF2VP16, a fusion between amino acids (aa) 1-91 of human MEF2D and aa 412-490 of the viral transcriptional activator VP16, was cloned into the pAdTrack-CMV viral shuttle vector (generously provided by Bert Vogelstein, Johns Hopkins University) and recombined in BJ5183 bacteria (Stratagene) to obtain E1-E3-deleted adenoviral bicistronic vectors to generate AdMEF2VP16, which expresses MEF2VP16 and GFP under separate CMV promoters. AdMEF2A, an adenovirus expressing both C-terminal FLAG-tagged human MEF2A and GFP, and AdGFP, a control virus expressing only GFP, were generated as described previously [6, 14]. Virus titers were determined in neonatal rat cardiomyocytes based upon GFP fluorescence and used at a multiplicity of infection (moi) of 1.0 or less when indicated.

Cell culture and transient transfection assays. Isolation and culture of neonatal rat ventricular cardiomyocytes was performed as described before in detail [15]. Low passage COS7 and HEK293 cells were grown in Dulbecco's modified Eagle's medium (Invitrogen) supplemented with 10% fetal bovine serum. NkL-TAg cells were cultured as described previously [16]. For transfection assays, cells were

grown in 48-well plates and transiently transfected using the indicated expression and reporter vectors with FuGENE 6 reagent (Roche) at 1.5 µl FuGENE:1 µg DNA ratios, and measured using the Dual Luciferase assay system (Promega), where *firefly* luciferase activity is normalized for *Renilla* luciferase activity to control for variations in transfection efficiency. For siRNA experiments, cardiomyocytes were transfected with control siRNAs or siRNAs specific for DMPK (Ambion) in a final concentration of 100 nM, using Oligofectamine (Invitrogen). Twenty-four hours after transfection, cells were washed in PBS and further treated as described.

Immunofluorescence and confocal microscopy. Cultured cardiomyocytes were fixed for 10 min in 4% paraformaldehyde and permeabilized with 0.2% Triton X-100 in PBS for 5 minutes. Primary and secondary antibodies were diluted using 1% BSA in TBS and incubations were carried out at room temperature for 1 hour. Cells were washed 3 times with PBS for 5 minutes, mounted with coverslips in 0.1 M Tris-HCl (pH 9.5)-glycerol (3:7) including 50 mg/ml *n*-propylgallate as anti-fading reagent, and analyzed by confocal microscopy using a Zeiss LSM 510 META instrument. Antibodies used included mouse anti α-actinin (Sigma, 1:500); rabbit anti α-actinin [17] (1:200), monoclonal anti-myomesin [17] (1:50), monoclonal anti-titin T12 [17]; rabbit anti-titin M8 [18] (1:50); monoclonal anti-EH-myomesin [19] (1:500); monoclonal anti-vinculin (Sigma, 1:50); Cy5 goat anti-rabbit and Cy3 goat anti-mouse (Jackson Immuno Research, 1:100 and 1:500, respectively); DAPI (1:100). Cell surface areas and cell length-width ratios were determined using SPOT-imaging software (Diagnostic Instruments).

RT-PCR. Total RNA was isolated from the indicated cell types using TRIzol reagent (Invitrogen). Three µg RNA was used as template for Superscript reverse transcriptase II (Gibco) using the indicated primer combinations (Table 1).

Western blot analysis. Protein was isolated from cells by lysis in extraction buffer (20 mM Tris (pH7.5), 150 mM NaCl, 1 mM EDTA, 1 mM EGTA, 1% Triton X-100, and complete protease inhibitor cocktail (Roche). Total protein from centrifuged lysate was separated by electrophoresis on a 10% SDS-PAGE gel and transferred to polyvinylidene difluoride membranes (Amersham Pharmacia Biotech). Antibodies used included mouse monoclonal anti-GFP (Santa Cruz, 1:500), mouse monoclonal anti-VP16 (Santa Cruz, 1:500), mouse monoclonal anti-FLAG (Sigma, 1:5000), and rabbit polyclonal anti-DMPK (Zymed, 1:500) in 10% non-fat dry milk, followed by corresponding horseradish peroxidase (HRP)-conjugated secondary antibodies (DAKO, 1:5000) and processed for chemiluminescent detection as described by the manufacturer (Amersham).

Generation of stable cardiac cell lines. NkL-TAg cells were cultured as described previously [16]. Double stable, MEF2VP16-inducible cells were generated using the T-REX system (Invitrogen) with modifications. Briefly, NkL-TAg cells were transfected using FuGENE 6 reagent (Roche) with 8 µg pCAgβTrs-

hygro, a vector expressing the Tet-repressor (TR) under control of a β-actin promoter (generously provided by Hans Clevers, Hubrecht Laboratory) and stable clones selected with 250 µg/µl hygromycin. Selected colonies were transiently transfected using FUGENE 6 reagent (Roche) with 0.2 µg pcDNA4/TO-luciferase (generously provided by Hans Clevers) to test their responsiveness to doxycyclin (Dox) using the Dual Luciferase assay system (Promega). Two different Tet-repressor clones (TR1 and TR4), showing high luciferase activity and low background, were subsequently transfected with 8.5 µg pcDNA4/TO-MEF2VP16 using FUGENE 6 reagent (Roche) and cultured in the presence of hygromycin and 750 µg/µl zeocin to generate double stable cell lines. Zeocin/hygromycin resistant clones were transiently transfected with a MEF2-luciferase reporter (3xMEF2-Luc [9]) to test their DOX-inducible MEF2 activation profile.

Agilent gene expression profiling and data analysis. TR1-194 and TR4-39 inducible MEF2VP16-NkL-TAg clones were maintained in parallel cultures, mortalized by overnight AdCre infection, cultured for an additional 3 days in serum-free media either in the presence or absence of 24 h Dox-treatment. Three corresponding cultures were pooled, total RNA extracted using TRIzol (Invitrogen) and cleaned with Qiagen RNeasy Mini Kits (Qiagen). RNA quantity was measured with a NanoDrop® ND-1000 UV-Vis Spectrophotometer (Wilmington), and RNA quality was monitored using an Agilent 2100 bioanalyzer. Agilent 44k mouse whole genome microarray slides (Palo Alto) were used and a dye-swap experimental design applied. RNA samples (500 ng each) acquired from the clones were amplified and labeled with Cy5- and Cy3-CTP (Perkin Elmer) to produce labeled cRNA using Agilent low RNA input fluorescent linear amplification kits following the manufacturer's protocol. After amplification and labeling, the dye-incorporation ratio was determined with NanoDrop® ND-1000 UV-Vis Spectrophotometer (Wilmington). For hybridization, the guidelines for 44k format arrays with cRNA targets were strictly followed. Briefly, 750 ng of Cy3-labeled cRNA and 750 ng Cy5-labeled cRNA were mixed and incubated with an Agilent microarray slide for 17 hours using an Agilent *in situ* hybridization kit following SSC buffer washing. The washed slides were immediately dried, and scanned using Agilent DNA Microarray Scanner (G2565BA). Raw data were generated using Agilent's Feature Extraction software (FE v7.1). Gene classifications were assigned based upon publicly available software and websites, including FATIGO Data mining with Ontology (www.fatigo.org), Mouse Genome Informatics (MGS; www.informatics.jax.org), GenBank and Medline.

Chromatin immunoprecipitation. Chromatin immunoprecipitation was carried out using the Upstate Biotechnology ChIP assay kit according to the manufacturer's instructions using anti-acetylated histone H3 antibody (Upstate Biotechnology) and pan-MEF2 polyclonal antibody (Santa Cruz). Equal amounts of soluble chromatin

from each sample were immunoprecipitated with 1 µg of the above mentioned antibodies. Following immunoprecipitation of immunocomplexes, the lysates were put at 65°C for four hours to reverse the formaldehyde crosslinking. Associated DNA was purified by phenol/chloroform extraction. PCR was carried out using specific primers to the promoter region of rat *dmpk* (FW: 5'- gagctattttggggtctctt, REV: 5'- cttcttcgtgactcagcaat).

Statistical analysis. The results are presented as means ± SEM. Statistical analyses were performed using INSTAT 3.0 software (GraphPad, San Diego) and Student's t-test or ANOVA followed by Tukey's post-test when appropriate. Statistical significance was accepted at a P value < 0.05.

RESULTS

Activation of MEF2 induces elongation in cultured cardiomyocytes

To address the role of MEF2 in cardiomyocyte remodeling, we first tested the efficiency of two different expression vectors of MEF2, one expressing wildtype MEF2A, and one expressing a constitutively active mutant of MEF2, MEF2VP16, using a luciferase reporter with 3 multimerized MEF2 binding sites upstream of a minimal TATA box (3xMEF2-Luc) as a readout in cotransfection experiments. Cotransfection of the reporter with MEF2A produced an approximate 12 ± 3-fold increase in luciferase activity. Even double amounts of MEF2A produced a similar activation profile of the reporter (15 ± 3) (Fig. 1A). In contrast, the MEF2VP16 expression vector resulted in a 134 ± 28-fold higher MEF2 transcriptional activity (Fig. 1A). These findings indicate that overexpression of wildtype MEF2A or MEF2VP16 will provide means to mimic either mild (MEF2A) or strong (MEF2VP16) activation of MEF2 transcription factors in cultured cardiomyoctes.

Figure 1. MEF2 induces eccentric cardiac hypertrophy. **A.** Cotransfection of 3xMEF2-Luc reporter with expression vectors for MEF2A (0.1 and 0.2 µg) and MEF2VP16 (0.1 µg) in COS7 cells, indicate that transcription is robustly activated by MEF2VP16. **B.** Schematic representation of the bicistronic adenoviral vectors expressing MEF2A and GFP or MEF2VP16 and GFP. **C.** Western blot analysis with either anti-FLAG and anti-GFP antibodies (upper panel) or anti-VP16 and anti-GFP antibodies (lower panel) on lysates of COS7 cells infected with AdMEF2A, or AdMEF2VP16 and AdGFP, respectively. **D.** Representative confocal images of immunostained cardiomyocytes infected with the indicated adenoviruses. Sarcomeric α-actinin staining demonstrates both hypertrophied (AdMEF2A and AdMEF2VP16) and thin and elongated (AdMEF2VP16) cells. Bar, 50 µm. **E.** Surface area measurements of cardiomyocytes (≥ 100 per experiment) infected with AdGFP, AdMEF2A and AdMEF2VP16. **F.** Quantitative examination of cell-length/cell-width ratios of cardiomyocytes (≥ 100 per experiment) infected with AdGFP, AdMEF2A and AdMEF2VP16. *Indicates P<0.05 compared to AdGFP infected cells.

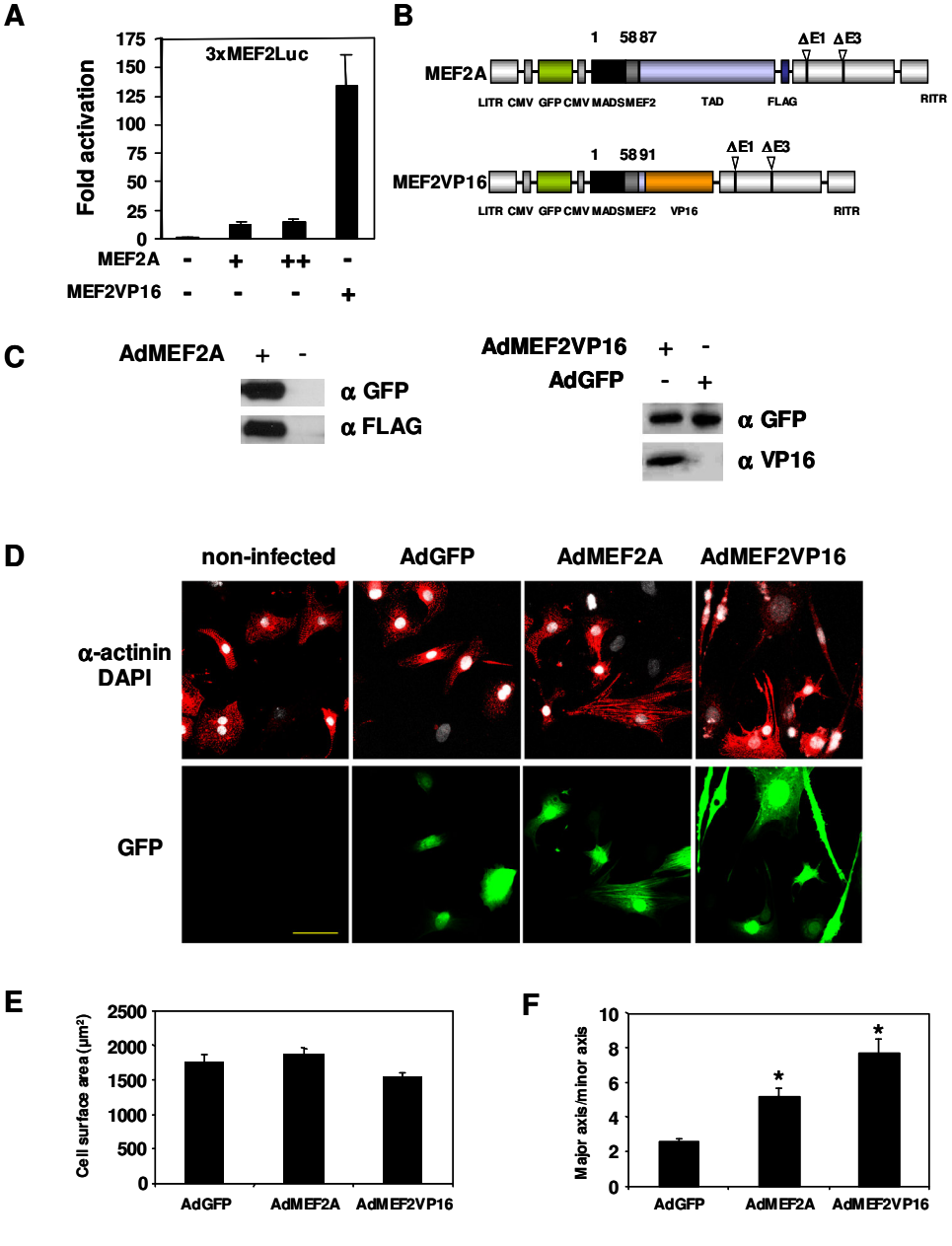
A
Fold activation
175
150
125
100
75
50
25
0
3xMEF2Luc
MEF2A - + ++ -
MEF2VP16 - - - +
B
MEF2A
1 58 87
ΔE1 ΔE3
LITR CMV GFP CMV MADS MEF2 TAD FLAG RITR
MEF2VP16
1 58 91
ΔE1 ΔE3
LITR CMV GFP CMV MADS MEF2 VP16 RITR
C
AdMEF2A + -
α GFP
α FLAG
AdMEF2VP16 + -
AdGFP - +
α GFP
α VP16
D
non-infected
AdGFP
AdMEF2A
AdMEF2VP16
α-actinin
DAPI
GFP
E
Cell surface area (μm²)
2500
2000
1500
1000
500
0
AdGFP
AdMEF2A
AdMEF2VP16
F
Major axis/minor axis
10
8
6
4
2
0
*
*
AdGFP
AdMEF2A
AdMEF2VP16

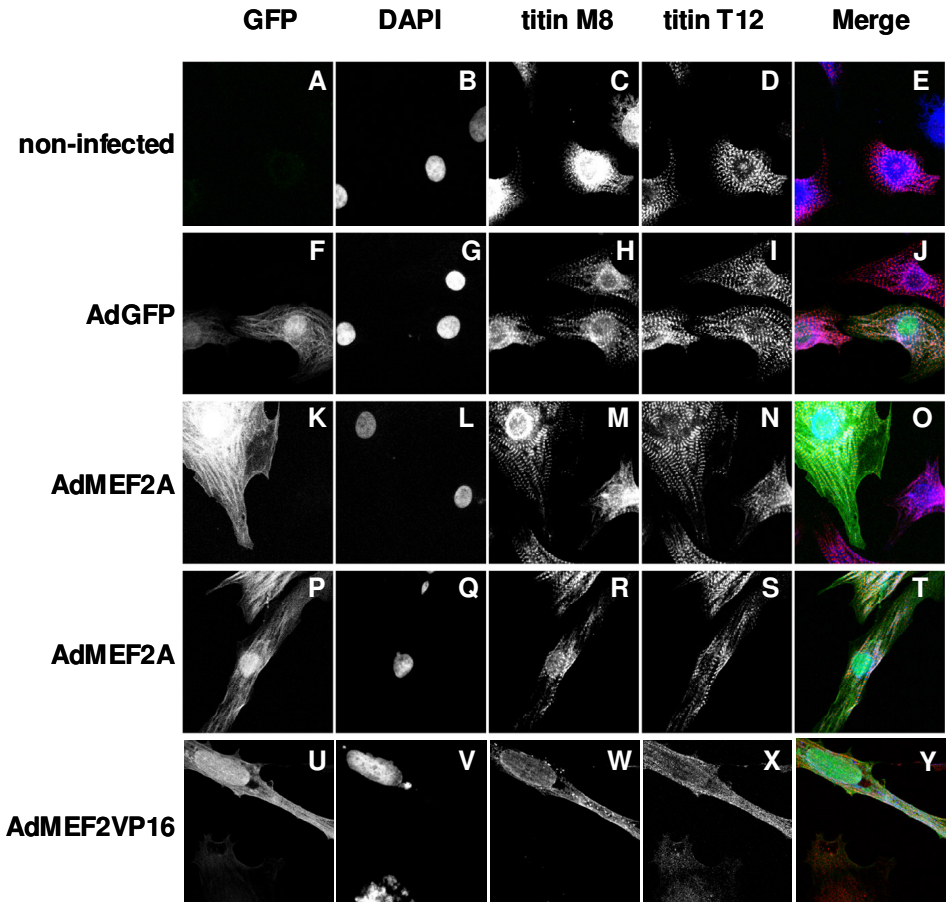

Figure 2. MEF2 activation promotes cardiomyocyte elongation. Confocal immunocytochemistry of cultured neonatal rat cardiomyocytes using antibodies raised against titin epitopes located in the Z-disc (titin T12) and in the M-band (titin M8), demonstrates that MEF2 stimulation preferentially stimulates myocyte elongation.

To overcome the low transfection efficiency of cultured cardiomyocytes, we generated adenoviral vectors to overexpress the two MEF2 constructs. Two replication-deficient, bicistronic adenoviruses were generated expressing either MEF2A and GFP or MEF2VP16 and GFP under control of separate CMV promoters (Fig. 1B). Western blotting with anti-GFP, anti-FLAG, and anti-VP16 antibodies confirmed that the viruses expressed proteins of the correct size (Fig. 1C). In contrast, the control AdGFP adenovirus only displayed immunoreactivity for GFP and not for FLAG (data not shown) or VP16 (Fig. 1C). The viruses were then

used to infect cultured neonatal rat ventricular myocytes. Following infection, cells were serum starved for 48 h, fixed and stained for α-actinin to identify cardiomyocytes and visualize myofibrils, and counterstained with DAPI to visualize nuclei (Fig. 1D). Control cells (uninfected or AdGFP infected) showed no signs of hypertrophy. Surprisingly, cardiomyocytes infected with AdMEF2A demonstrated different phenotypes: the majority of GFP-positive cells were elongated when compared to control cells, and less than 10% of GFP-positive cells were visibly larger than control cells. Of note, the larger cells did not display the typical features of hypertrophied cells, including sarcomere assembly, vigorous beating, or ANF positivity (data not shown). AdMEF2VP16-infected cells showed a more pronounced elongation by 48 hours, and larger cells were only sporadically detected in these cultures. In line, AdMEF2A- and AdMEF2VP16-infected cultures did not reveal a significant increase in average cell surface area (1870 ± 93 μm^2 and 1539 ± 74 μm^2, respectively), a measure of hypertrophy, as compared to AdGFP-infected cultures (1778 ± 94 μm^2) (Fig. 1E). We next determined the ratio of the length of the major and minor axis of cells in our experimental groups, as a measure of cellular elongation. AdGFP-infected cardiomyocytes had a ratio of 2.57 ± 0.16, while AdMEF2A- and AdMEF2VP16-infected cells displayed a 2- and 3 fold increase in major to minor axis ratios (5.20 ± 0.50 and 7.70 ± 0.77, respectively; $P < 0.05$) compared to AdGFP-infected cells (Fig. 1F). Combined, these data suggest that neither a mild increase in MEF2 transcriptional activity in cultured cardiomyocytes, accomplished by AdMEF2A infection, nor a high increase in transcriptional activity of MEF2, by AdMEF2VP16 infection, provoke a classical hypertrophic response, but rather promotes elongation of cardiomyocytes.

MEF2 activation in cardiomyocytes causes loss of myofibril architecture

To more accurately analyze the phenotypes we observed upon AdMEF2A and AdMEF2VP16 infection, we immunostained for specific intracellular components of cardiomyocytes and performed confocal microscopy at higher magnification (Fig. 2). Cells were either left uninfected (Fig. 2A-E), infected with AdGFP (Fig. 2F-J), AdMEF2A (Fig. 2K-T), or AdMEF2VP16 (Fig 2. U-Y) at moi's <1, to be able to identify infected cells (GFP-positive) adjacent to non-infected cells within the same cultures. Fluorescence for GFP was used to track the individual cells infected with AdGFP, AdMEF2A or AdMEF2VP16 (Fig. 2, Panels A, F, K, P and U). DAPI staining was used to visualize nuclei (Fig. 2, Panels B, G, L, Q, V). We immunostained cells for either titin at the M-band (titin M8; Fig. 2, Panels C, H, M, R, W) or titin at the Z-disc (titin T12; Fig. 2, Panels D, I, N, S, X), and finally merged the different channels (Fig. 2, Panels E, J, O, T, Y).

AdGFP-infected cells cultured under serum free conditions displayed a regular pattern of myofibril staining, with a regular spacing between the M-band and the Z-

disc (Fig. 2J), which was indistinguishable from non-infected cells (Fig. 2E and J). As discussed above, upon AdMEF2A infection two different phenotypes were distinguishable, either elongated cells or enlarged cells that did not show signs of classical cardiomyocyte hypertrophy. Fig. 2O displays a representative example of an AdMEF2A-infected enlarged myocyte, with adjacent, non-infected, significantly smaller cardiomyocytes in the same culture. In the larger AdMEF2A-infected cells, myofibril structures were less well organized (Fig. 2M, N, O). In elongated AdMEF2A-infected myocytes, the organization of M-band and Z-disc structures were even less apparent (Fig. 2R, S), resulting in overall poorly defined myofibrils (Fig. 2T). The most dramatic loss of sarcomeres was evident in AdMEF2VP16-infected cultures, with only remnants of M-band (Fig. 2W) and Z-disc structures (Fig. 2X).

Next, we inspected cardiomyocyte cultures with altered MEF2 transcriptional activity for other myofibril components; α-actinin at the Z-disc, and myomesin located at the M-band (Fig. 3). Cells were left uninfected (Fig. 3A-E), infected with AdGFP (Fig. 3F-J), AdMEF2A (Fig. 3K-T), or AdMEF2VP16 (Fig. 3U-Y). Fluorescence for GFP was used to track the individual cells infected with AdGFP, AdMEF2A or AdMEF2VP16 (Fig. 3, Panels A, F, K, P, and U). DAPI staining was used to visualize nuclei (Fig. 3, Panels B, G, L, Q, and V). Examples of cells immunostained for either α -actinin at the Z-disc (Fig. 3, Panels C, H, M, R, W) or myomesin at the M-band (Fig. 3, Panels D, I, N, S, X), and merged channels (Fig. 3, Panels E, J, O, T, Y) are presented. Uninfected or AdGFP-infected cultures demonstrated a regular pattern of sarcomere staining (Fig. 3E, J). Enlarged AdMEF2A-infected cells demonstrated slightly less well-defined myofibril integrity (Fig. 3O) or more severely affected organization of myomesin (Fig. 3T), while elongated AdMEF2VP16-infected cells showed only remnants of either myofibril structure (arrows in Fig. 3S, W, X).

In conclusion, these data demonstrate that increased MEF2 transcriptional activity in cultured cardiomyocytes provokes myocyte elongation, accompanied by a progressive loss of myofibrillar structures.

Inducible activation of MEF2 in cardiac cell lines

To begin to understand the mechanisms underlying the characteristic phenotypic alterations presumably evoked by MEF2 transcriptional activity and activation of its downstream target genes, we generated a cellular system to inducibly activate MEF2 target genes in NkL-TAg cells, a previously described ventricular muscle cell line [16]. To this end, NkL-TAg cells were stably transfected with an expression vector harboring the Tet-repressor (TR) under control of a β-actin promoter using hygromycin as selectable marker (Fig 4A). About 80 clones were obtained and tested for Dox-inducibility after transient transfection of a

luciferase reporter construct downstream of two Tet-operator (TetO) sites (Fig. 4B). We continued with 2 NkL-TAg-TR clones (designated TR1 and TR4), which showed at least a 100-fold increase of luciferase activity in the presence of Dox and background luciferase in the absence of Dox (Fig. 4B).

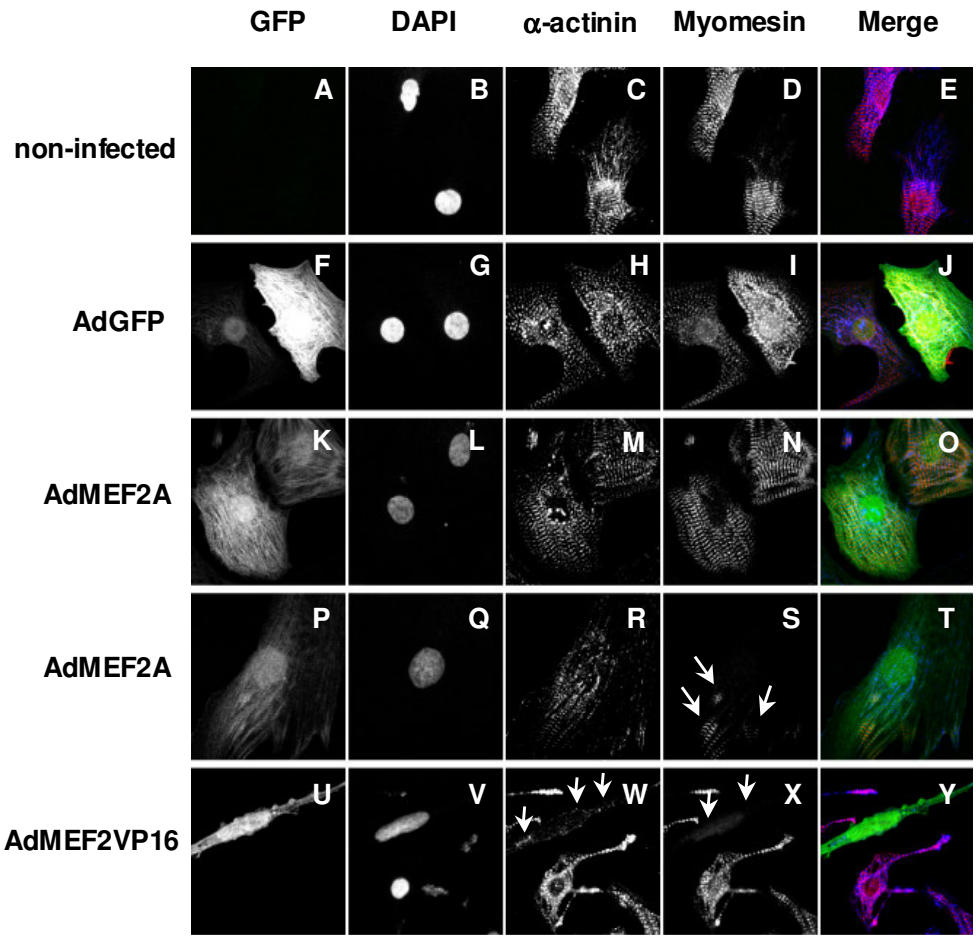

Figure 3. MEF2 activation promotes sarcomere degeneration. Confocal immunocytochemistry of cultured neonatal rat cardiomyocytes, using anti-sarcomeric α-actinin (Z-disc) and anti-myomesin (M-band) antibodies, demonstrates that MEF2-induced myocyte elongation is accompanied with myofibril degeneration. Arrows in Panels S, W and X point to residual α-actinin immunoreactivity.

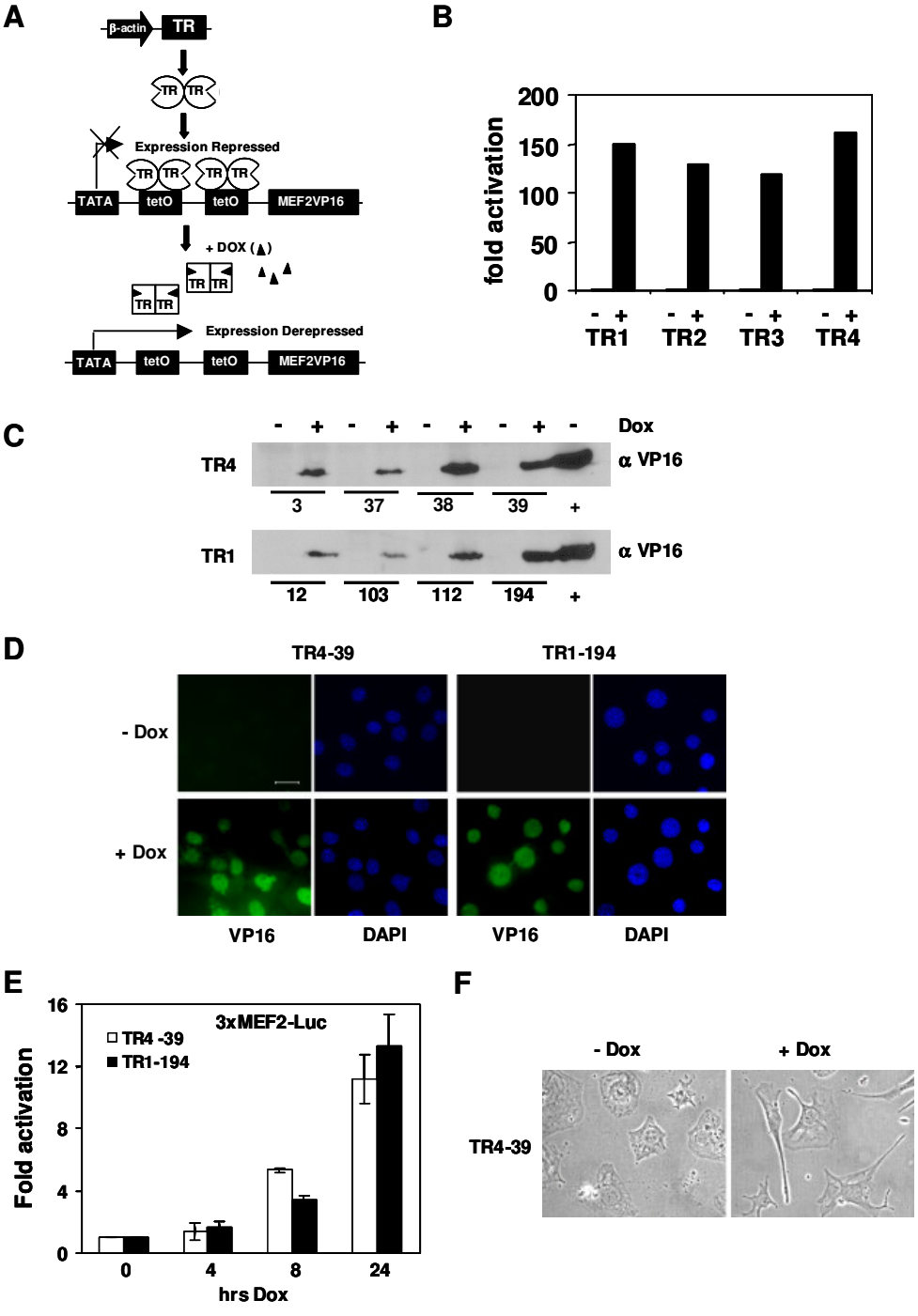
A
β-actin
TR
TR TR
Expression Repressed
TR TR TR TR
TATA
tetO
tetO
MEF2VP16
+ DOX (▲)
TR TR
TR TR
Expression Derepressed
TATA
tetO
tetO
MEF2VP16
B
fold activation
200
150
100
50
0
- + - + - + - +
TR1 TR2 TR3 TR4
C
- + - + - + - + -
Dox
TR4
α VP16
3 37 38 39 +
TR1
α VP16
12 103 112 194 +
D
TR4-39
TR1-194
- Dox
+ Dox
VP16 DAPI VP16 DAPI
E
Fold activation
16
12
8
4
0
3xMEF2-Luc
TR4 -39
TR1-194
0 4 8 24
hrs Dox
F
- Dox
+ Dox
TR4-39

Next, we stably transfected TR1 and TR4 clones with a construct harboring MEF2VP16 under transcriptional control of 2 TetO sites (Fig. 4A), using zeocin as a selectable marker. Up to 200 clones were obtained and tested for inducible MEF2 transcriptional activity following Dox stimulation using a 3xMEF2-Luc reporter (data not shown). For both TR1 and TR4, 4 double-stable clones were obtained which only expressed MEF2VP16 after Dox stimulation, as demonstrated by Western blotting using an antibody against VP16 (Fig. 4C). To control for cell-based variations, we selected two TR-MEF2VP16 clones, designated TR1-194 and TR4-39, for further analysis.

Immunofluorescent staining showed absence of VP16 immunofluorescence in the absence of Dox, and homogenous MEF2VP16 expression after 24 h induction with Dox, which was exclusively localized to the nucleus, as expected for a constitutively active MEF2 transcription factor (Fig. 4D). Finally, both clones were transiently transfected with 3xMEF2-Luc, mortalized with AdCre infection [16], cultured for 72 hrs in serum free media to allow to adopt a ventricular muscle cell fate, and exposed to Dox for varying periods to establish at which time-course elevated MEF2 transcriptional activity was evident. In both clones, an approximate 5-fold increase of MEF2 transcriptional activity was evident at 8 h, compared to TR1-194 and TR4-39 clones cultured in the absence of Dox (Fig. 4E). After 24 h Dox exposure, both clones demonstrated an approximate 10-fold increase in MEF2 transcriptional activity (Fig. 4E). Both TR1-194 and TR4-39 cell lines elongated after Cre-induced mortalization and Dox stimulation (Fig. 4F, and data not shown).

In conclusion, we established a novel system that allows inducible activation of MEF2 transcriptional activity in ventricular muscle cells by addition of doxycyclin to the culture medium.

Figure 4. Generation of cardiac cell lines inducibly expressing MEF2VP16. **A.** Schematic representation of double-stable cell line expressing MEF2VP16 after Dox stimulation. **B.** Stable cell lines expressing the Tet repressor (TR) were tested for Dox-inducibility, using a luciferase reporter downstream of Tet operators. **C.** Western blot analysis, using anti-VP16 antibody, on lysate of different double stable TR-MEF2VP16 clones, which are either untreated or stimulated with Dox for 24 h. All clones express MEF2VP16 only after stimulation with Dox. Pos.ctrl, Western blot positive control for VP16 antibody **D.** Immunofluorescent staining of TR4-39 and TR1-194 cells show homogenous expression of MEF2VP16 after induction with Dox. Note that MEF2VP16 is localized primarily to the nuclei of cells. Bar, 20 µm. **E.** Luciferase measurements on TR4-39 and TR1-194 cells, transiently transfected with 3xMEF2Luc reporter, indicate a time-dependent increase in MEF2 transcriptional activity after stimulation with Dox. **F.** Bright field microscopic images showing elongation of TR4-39 cells after Dox stimulation.

Cardiac genes regulated by MEF2

Both inducible MEF2VP16 ventricular myocyte cell lines were used for a genome-wide microarray analysis using Agilent mouse chips containing 44,000 genes, to identify the earliest gene expression pattern regulated by the transcription factor MEF2, as the morphological alterations in AdMEF2VP16-infected cardiomyocytes were already evident by 24-48 hrs. TR1-194 and TR4-39 cells were plated in parallel cultures, mortalized by overnight infection with AdCre, cultured in SF medium for 72 hrs, and cultured for an additional 24 hrs in the absence or presence of Dox. 75 genes (0.2% of all genes) were differentially expressed in both TR1-194 and TR4-39 cells with a fold change in expression ≥ 2 ($P < 0.01$) (Table 2). Among these 75 genes, 43 showed an increase in expression, 32 genes a decreased expression. We were interested to identify genes that may provide explanations for the dramatic change in morphology we observed in cultured cardiomyocytes with altered MEF2 transcriptional activity. Gene ontology classifications revealed an overrepresentation of genes in three specific subclasses: cell-matrix adhesion, cytoskeletal remodeling, and energy metabolism (Table 2, Fig. 5A). We picked 10 genes from the most interesting classifications to verify differential expression by RT-PCR (Fig. 5B). For example*, integrin alpha-7* (Itga7), *nexilin* (Nexn), *connective tissue growth factor* (CTGF), *regulatory myosin light chain 9* (Myl9), *myotonic dystrophy protein kinase* (DMPK), *sarcoglycan alpha* (Sgca) and *sarcoglycan beta* (Sgcb) were each significantly upregulated upon MEF2VP16 expression in TR1-194 and TR4-39 clones (Fig. 5B). In contrast, *integrin beta 4* (Itgb4), *glutathione S-transferase alpha 1* (gsta1) and *mucin 5* (muc5b) were significantly downregulated. Another gene class differentially regulated by MEF2 transcription factors included genes involved in energy metabolism and mitochondrial energy production. This is in line with previous reports suggesting a direct or indirect role for MEF2 to control cardiac energy production [10, 20]. Combined, these data indicate that MEF2 activity activates subsets of genes primarily localized to or functioning at the cytoskeleton, focal adhesion sites, the extracellular matrix, and energy metabolism/mitochondrial energy production.

Figure 5. Classification of MEF2 target genes. **A.** Bar graph indicating the number of differentially expressed genes in different functional classifications. **B.** Semi-quantitative RT-PCR for mRNA levels of indicated genes in TR1-194 and TR4-39 clones in absence or presence of Dox. Ribosomal protein L7 mRNA levels were determined as control for equal amplification and loading. **C-V.** Confocal immunocytochemistry of cultured neonatal rat cardiomyocytes, using anti-EH-myomesin and anti-vinculin antibodies, demonstrates that MEF2 activation alters the distribution of focal adhesion sites. Arrows in Panel S point to residual myomesin immunoreactivity.

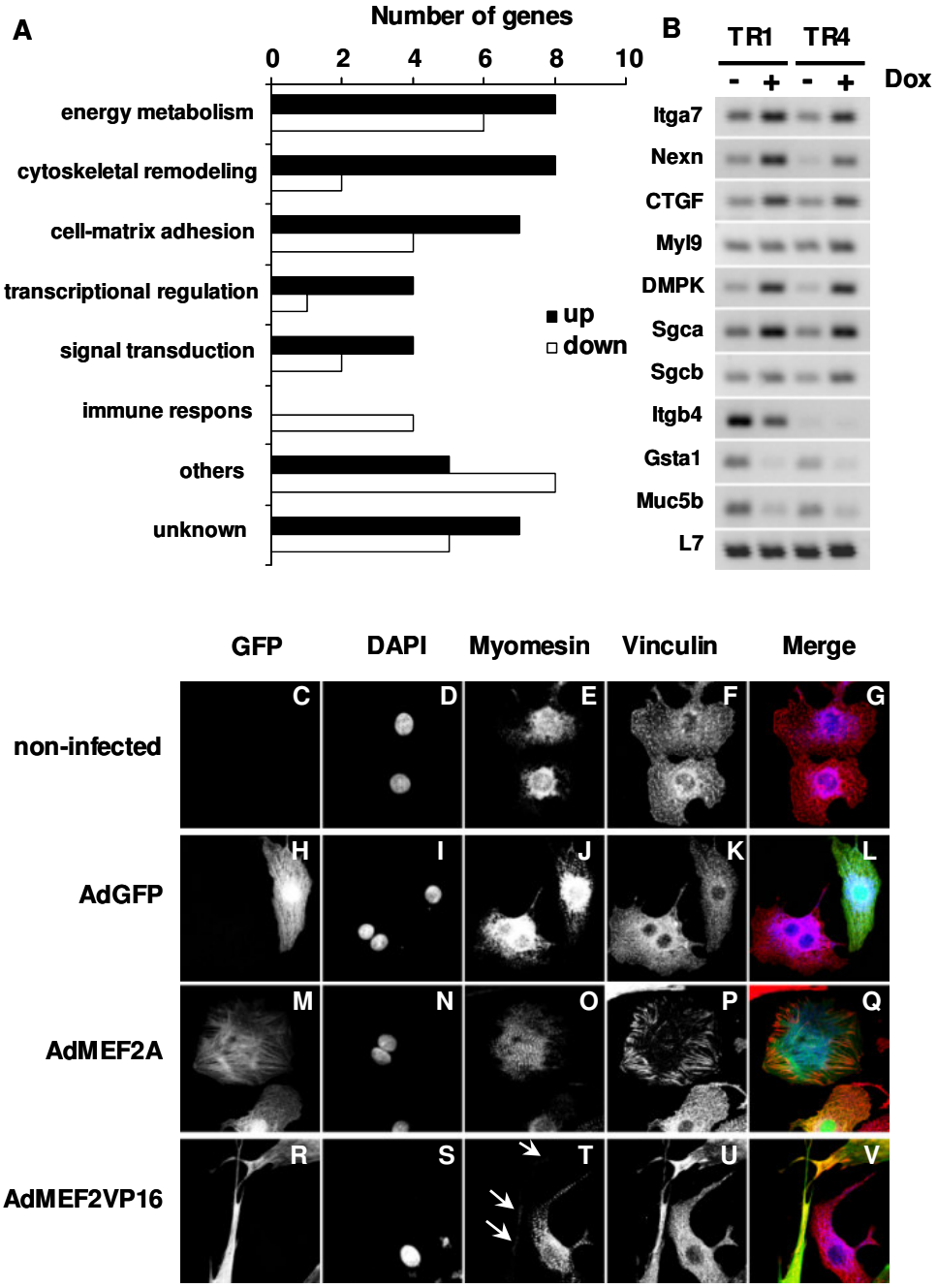
A
Number of genes
0
2
4
6
8
10
energy metabolism
cytoskeletal remodeling
cell-matrix adhesion
transcriptional regulation
signal transduction
immune respons
others
unknown
up
down
B
TR1
TR4
- + - +
Dox
Itga7
Nexn
CTGF
Myl9
DMPK
Sgca
Sgcb
Itgb4
Gsta1
Muc5b
L7
GFP
DAPI
Myomesin
Vinculin
Merge
non-infected
AdGFP
AdMEF2A
AdMEF2VP16
C
D
E
F
G
H
I
J
K
L
M
N
O
P
Q
R
S
T
U
V

Table 2. Functional clustering of genes regulated by MEF2.

Accesion Number	Gene	Description	Fold Change TR1-194	Fold Change TR4-39
Cell-matrix adhesion (11)				
NM_010217	CTGF	connective tissue growth factor	10,5	3,6
NM_008398	Itga7	integrin alpha 7	7,3	4,1
NM_199465	Nexn	nexilin	4,8	4,4
NM_009621	Adamts1	disintegrin-like and metalloprotease (reprolysin type) with thrombospondin type 1 motif, 1	3,9	5,0
NM_013494	Cpe	carboxypeptidase E	2,1	3,7
NM_011580	Thbs1	thrombospondin 1	2,9	2,2
NM_144862	Lims2	LIM and senescent cell antigen like domains 2	2,5	2,3
BC059192	Itgb4	integrin beta 4	-2,6	-2,2
NM_011595	Timp3	tissue inhibitor of metalloproteinase 3	-2,6	-2,5
NM_054077	Prelp	proline arginine-rich end leucine-rich repeat	-4,1	-2,7
AF064749	Col6a3	type VI collagen alpha 3 subunit	-4,0	-4,3
Cytoskeleton (10)				
BC055439	Myl9	myosin, light polypeptide 9, regulatory	10,2	7,0
NM_009606	Acta1	actin, alpha 1, skeletal muscle	13,4	2,6
S60315	DMPK	myotonic dystrophy kinase	3,9	4,0
NM_011619	Tnnt2	troponin T2, cardiac	2,9	3,3
NM_009161	Sgca	sarcoglycan, alpha (dystrophin-associated glycoprotein)	3,5	2,5
NM_011890	Sgcb	sarcoglycan, beta (dystrophin-associated glycoprotein)	2,7	2,9
NM_013560	Hspb1	heat shock protein 1	3,0	2,5
NM_008800	Pde1b	phosphodiesterase 1B, Ca2+-calmodulin dependent	2,4	2,2
AK034012	Synpo	RIKEN clone:9330140I15	-2,1	-2,3
U72681	Vill	EF-6	-2,2	-2,2
Energy metabolism (14)				
NM_009943	Cox6a2	cytochrome c oxidase, subunit VI a, polypeptide 2	13,8	3,9
NM_021273	Ckb	creatine kinase, brain	3,0	3,3
NM_007431	Akp2	alkaline phosphatase 2, liver	3,0	3,3
NM_008509	Lpl	lipoprotein lipase	2,5	3,2
NM_024188	Oxct1	3-oxoacid CoA transferase 1	2,8	2,8
NM_026619	1700020F09Rik	RIKEN cDNA 1700020F09 gene	2,5	2,5
NM_007382	Acadm	acetyl-Coenzyme A dehydrogenase, medium chain	2,3	2,4
NM_007808	Cycs	cytochrome c, somatic	2,0	2,2
NM_010795	Mgat3	mannoside acetylglucosaminyltransferase 3	-2,7	-2,1
NM_010358	Gstm1	glutathione S-transferase, mu 1	-2,8	-2,6
NM_010359	Gstm3	glutathione S-transferase, mu 3	-3,5	-2,3
NM_011921	Aldh1a7	aldehyde dehydrogenase family 1, subfamily A7	-3,6	-2,4
NM_007436	Aldh3a1	aldehyde dehydrogenase family 3, subfamily A1	-5,5	-6,6
NM_008181	Gsta1	glutathione S-transferase, alpha 1 (Ya)	-8,7	-8,0
Signal transduction (6)				
AK004534	Rasl11b	RIKEN clone:1190017B18	2,7	3,3
AK033726	Map3k5	mitogen activated protein kinase kinase kinase 5	2,9	2,2
XM_355574	Gnai1	guanine nucleotide binding protein, alpha inhibiting 1	2,1	2,9
NM_026505	Bambi	BMP and activin membrane-bound inhibitor	2,5	2,4
NM_009368	Tgfb3	transforming growth factor, beta 3	-3,2	-2,1
NM_181748	Gpr120	G protein-coupled receptor 120	-2,7	-2,8
Transcriptional regulation (5)				
NM_017373	Nfil3	nuclear factor, interleukin 3, regulated	3,4	3,2
NM_025926	Dnajb4	DnaJ (Hsp40) homolog, subfamily B, member 4	2,4	3,4
NM_011600	Tle4	transducin-like enhancer of split 4	2,5	2,5
NM_011542	Tcea3	transcription elongation factor A (SII), 3	2,3	2,2
NM_010495	Idb1	inhibitor of DNA binding 1	-3,6	-2,9

Immune response (4)				
NM_010741	Ly6c	lymphocyte antigen 6 complex, locus C	-2,4	-2,3
NM_010779	Mcpt4	mast cell protease 4	-3,9	-3,0
NM_011333	Ccl2	chemokine (C-C motif) ligand 2	-7,0	-2,7
NM_020519	1110021N19Rik	RIKEN cDNA 1110021N19 gene	-4,9	-5,3
Others (13)				
NM_008871	Serpine1	serine (or cysteine) proteinase inhibitor, clade E, member 1	2,5	3,3
NM_153098	Cd109	CD109 antigen (Cd109)	2,0	3,8
NM_024185	2310047O13Rik	RIKEN cDNA 2310047O13 gene	2,0	2,9
NM_029508	0610009F02Rik	RIKEN cDNA 5830443C21 gene	2,0	2,3
NM_146194	Picalm	phosphatidylinositol binding clathrin assembly protein (Picalm)	2,1	2,1
NM_009115	S100b	S100 protein, beta polypeptide, neural	-2,9	-2,2
NM_030261	Sesn3	sestrin 3	-3,2	-2,0
NM_013568	Kcna6	potassium voltage-gated channel, shaker-related, subfamily, member 6	-3,4	-2,8
AK041604	Dact2	RIKEN clone:A630024E20	-3,9	-2,5
NM_030127	Htra3	RIKEN cDNA 9530081K03 gene	-5,2	-2,1
NM_008597	Mglap	matrix gamma-carboxyglutamate (gla) protein	-5,0	-3,5
NM_019414	Selenbp2	selenium binding protein 2	-5,9	-4,9
NM_028801	Muc5b	mucin 5, subtype B, tracheobronchial	-13,5	-11,9
Unknown (12)				
AK086025	4631423F02Rik	RIKEN clone:D830045N18	6,9	2,3
AK017206	5033430I15Rik	RIKEN clone:5033430I15	4,6	3,2
NM_026931	1810011O10Rik	RIKEN cDNA 1810011O10 gene	4,3	3,2
NM_145980	8430408G22Rik	RIKEN cDNA 8430408G22 gene	2,2	4,2
NM_173752	1110067D22Rik	RIKEN cDNA 1110067D22 gene	2,8	2,9
AK008679	2210008N01Rik	RIKEN clone:2210008N01	2,7	2,4
AK01525	4930431B09Rik	RIKEN clone:4930431B09	2,2	2,6
AK021294	2810416G20Rik	RIKEN clone:D530019O13	-2,2	-2,2
NM_178642	AU040576	expressed sequence AU040576	-2,5	-2,0
NM_027950	1700012B18Rik	RIKEN cDNA 1700012B18 gene	-2,2	-2,9
NM_026821	D4Bwg0951e	DNA segment, Chr 4	-2,8	-2,4
AA726875	AA726875	cDNA clone IMAGE:1193490	-4,5	-2,3

MEF2 activation alters focal adhesion structures in cardiomyocytes

To verify whether alterations in cellular adhesion indeed correlated with the elongation of cultured cardiomyocytes upon MEF2 activation, we infected cardiomyocytes with AdMEF2A and AdMEF2VP16 and immunostained cultures for EH-myomesin and vinculin, a component of cardiac focal adhesion sites. Cells were left uninfected (Fig. 5C-G), infected with AdGFP (Fig. 5H-L), AdMEF2A (Fig. 5M-Q), or AdMEF2VP16 (Fig. 5R-V). Fluorescence for GFP was used to track the individual cells infected with AdGFP, AdMEF2A or AdMEF2VP16 (Fig. 5, Panels C, H, M, and R). DAPI staining was used to visualize nuclei (Fig. 5, Panels D, I, N, S). Examples of cells immunostained for either EH-myomesin at the M-band (Fig. 5, Panels E, J, O, T) or vinculin to visualize the localization of focal adhesions (Fig. 5, Panels F, K, P, U), and merged channels (Fig. 5, Panels G, L, Q, V) are presented. Uninfected or AdGFP-infected cultures demonstrated a regular pattern of sarcomere staining (Fig. 5D, I) and a punctuate distribution of vinculin at the focal

adhesions (Fig. 5E, J). Enlarged AdMEF2A-infected cells with modestly impaired myofibril integrity, displayed a redistribution of vinculin towards the outer borders of cells (Fig. 5N). Highly elongated AdMEF2VP16-infected cells with only remnants of myofibrillar structure (Arrows in Fig. 5S), demonstrated intense vinculin staining at the most distal tips of their cellular structure.

Thus, increased MEF2 transcriptional activity in cultured cardiomyocytes activates a gene program associated with a gradual loss of myofibrillar structure, which is accompanied by an increase and redistribution of focal adhesion sites.

DMPK is a cardiac MEF2 target gene

Of all genes found to be upregulated by MEF2 activation, DMPK was of specific interest. DMPK has initially been implicated in myotonic dystrophy (DM), an inherited degenerative neuromuscular disorder [21-24]. DM patients suffer from skeletal muscle myotonia, muscle weakness, and cardiac conduction defects. Furthermore, transgenic mice overexpressing DMPK display a heart failure phenotype, with extensive myocyte disarray and interstitial fibrosis [25].

To verify that DMPK represents a direct transcriptional target of MEF2, rat, mouse and human orthologs were aligned and analyzed for conserved MEF2 binding sites. One conserved MEF2 binding sequence (CTAAATTTAA) was detected 513 bp upstream of the transcriptional start site of the rat *dmpk* gene (Fig. 6A). We performed ChIP analysis to determine whether MEF2 binds to this A/T rich motif (Fig. 6B). Chromatin was immunoprecipitated from rat neonatal cardiomyocytes infected with either AdGFP or AdMEF2A, using antibodies directed against MEF2 and acetylated histone H3. No antibody immunoprecipitates were used as negative control. PCR amplification of the immunoprecipitated material using primers flanking the MEF2 site, demonstrate MEF2 binding to the *dmpk* promoter in cardiomyoctes infected with the MEF2A expressing adenovirus (Fig. 6B).

Figure 6. MEF2 induces cardiomyocyte elongation via DMPK. **A.** Sequence alignment of rat, mouse, and human *dmpk* promoter regions. The gray box indicates the conserved -513 MEF2 site. **B.** ChIP analysis was performed by PCR using primers flanking the MEF2 site on chromatin immunoprecipitated using either a MEF2 or an acetylated histone H3 antibody. No antibody immunoprecipitations serve as negative control, non-immunoprecipitated DNA was used as input control. **C.** Western blot analysis for DMPK expression in cardiomyocytes pre-transfected with either control or DMPK specific siRNAs and infected with the indicated adenoviruses. Immunoreactivity for GAPDH serves as loading control. **D.** Graph indicating the percentage of cardiomyocytes, pre-transfected with either control or DMPK specific siRNAs and infected with the indicated adenoviruses, with a major axis/minor axis ratio <2.5, between 2.5 and 5, or >5. **E.** Confocal immunocytochemistry of cultured neonatal rat cardiomyocytes, using an anti-α-actinin antibody, demonstrates that knockdown of DMPK inhibits MEF2 induced cardiomyocyte elongation. Arrows point to residual α-actinin immunoreactivity.

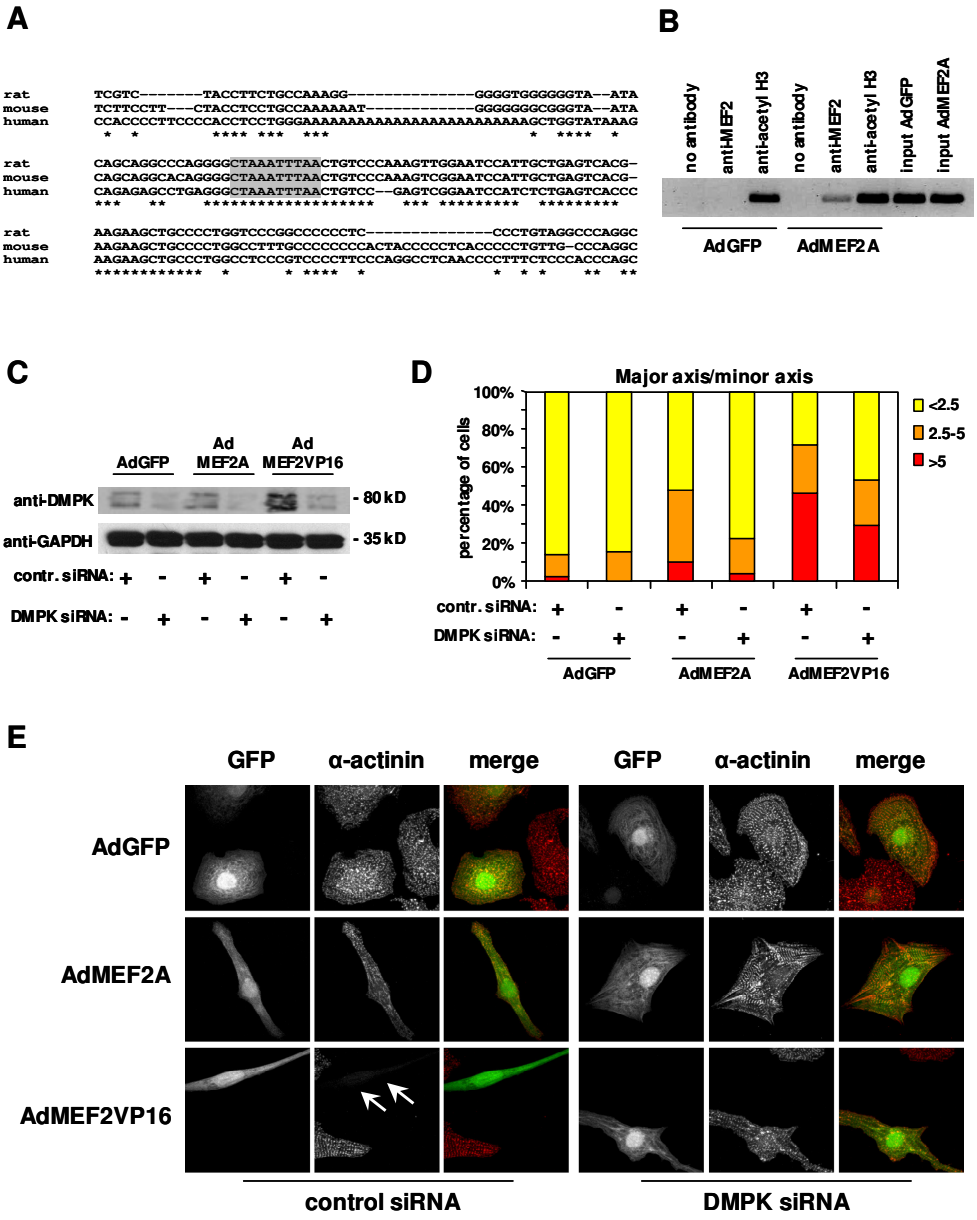
A
rat TCGTC--------TACCTTCTGCCAAAGG----------GGGGTGGGGGGTA--ATA
mouse TCTTCCTT---CTACCTCCTGCCAAAAAAT----------GGGGGGGCGGGTA--ATA
human CCACCCCTTCCCCACCTCCTGGGAAAAAAAAAAAAAAAAAAAAAAAAAAGCTGGTATAAAG
rat CAGCAGGCCCAGGGGCTAAATTTAACTGTCCCAAAGTTGGAATCCATTGCTGAGTCACG-
mouse CAGCAGGCACAGGGGCTAAATTTAACTGTCCCAAAGTCGGAATCCATTGCTGAGTCACG-
human CAGAGAGCCTGAGGGCTAAATTTAACTGTCC--GAGTCGGAATCCATCTCTGAGTCACCC
rat AAGAAGCTGCCCCTGGTCCCGGCCCCCCTC----------CCCTGTAGGCCCAGGC
mouse AAGAAGCTGCCCCTGGCCTTTGCCCCCCCCACTACCCCCTCACCCCCTGTTG-CCCAGGC
human AAGAAGCTGCCCTGGCCTCCCGTCCCCTTCCCAGGCCTCAACCCCTTTCTCCCACCCAGC
B
no antibody
anti-MEF2
anti-acetyl H3
no antibody
anti-MEF2
anti-acetyl H3
input AdGFP
input AdMEF2A
AdGFP
AdMEF2A
C
AdGFP
Ad MEF2A
Ad MEF2VP16
anti-DMPK
- 80 kD
anti-GAPDH
- 35 kD
contr. siRNA: + - + - + -
DMPK siRNA: - + - + - +
D
Major axis/minor axis
percentage of cells
100%
80%
60%
40%
20%
0%
<2.5
2.5-5
>5
contr. siRNA: + - + - + -
DMPK siRNA: - + - + - +
AdGFP
AdMEF2A
AdMEF2VP16
E
GFP
α-actinin
merge
GFP
α-actinin
merge
AdGFP
AdMEF2A
AdMEF2VP16
control siRNA
DMPK siRNA

DMPK upregulation is required for MEF2-induced myocyte elongation

In order to assess the potential role of DMPK in MEF2 induced cardiomyocyte remodeling, we evaluated the effect of DMPK siRNA knockdown during this remodeling process. As determined by Western blotting, we established significant knockdown of DMPK expression levels by transfecting cardiomyocytes with siRNAs directed against DMPK (Fig. 6C). Infection with AdMEF2A and especially AdMEF2VP16 enhanced DMPK protein levels in cardiomyocytes pre-transfected with control siRNA. This increase in expression, however, was inhibited in cardiomyocytes pre-transfected with siRNA targeting DMPK, where DMPK expression levels were comparable to the basal expression level (Fig. 6C).

Next, we investigated the effect of DMPK inhibition on MEF2 induced cardiomyocyte elongation by determination of the ratio of the length of the major and minor axis of the cells. Pre-transfection with control siRNA had no effect on cellular morphology (data not shown). MEF2 activation induced elongation of cardiomyocytes transfected with control siRNA as the percentage of GFP positive cells with a major axis/minor axis ratio >5 amounted to 10.4% and 46% after infection with AdMEF2A and AdMEF2VP16, compared to 2.5% for AdGFP infected control cells (Fig. 6D). Cardiomyocytes pre-transfected with DMPK siRNA showed a significant attenuation of the elongation response, as the percentage of GFP positive cells with a major axis/minor axis ratio >5, declined to 3.5%, 28.9%, and 0%, for AdMEF2A, AdMEF2VP16, and AdGFP infected cells, respectively (Fig. 6D). Representative images of cardiomyocytes pre-transfected with either control or DMPK siRNA and infected with AdGFP, AdMEF2A, or AdMEF2VP16, and immunostained for α-actinin are given in Figure 6E. Noteworthy, sarcomeric degeneration seemed to be less pronounced after knockdown of DMPK expression. Conclusively, DMPK is a direct cardiac target gene of MEF2 and promotes elongation of cardiomyocytes.

DISCUSSION

One pivotal observation of this study is that MEF2 activity in postnatal cardiac muscle promotes changes that are consistent with the development of dilated cardiomyopathy. The activation of a “fetal” gene program is a highly conserved feature of the hypertrophic response and has been extensively studied as a means to identify physiological regulators of hypertrophy. Although the initial steps of the induction of embryonic genes are reversible, chronic changes in the cardiac gene program may trigger pathological changes in the myocardium that can be irreversible in nature and promote cardiac dysfunction. Dilation of the ventricular chamber and the associated increase in stress on the ventricular wall are often the

first irreversible steps towards heart failure [26]. Accordingly, the transcription factors and their target genes that connect biomechanical forces and the activation of stress pathways to morphological changes of the myocardium are central to understanding the initiation and progression of heart failure.

Using a multidisciplinary approach, we analyzed the consequences of activating the transcription factor MEF2 in cardiac muscle. As described earlier, MEF2 promotes cardiomyopathic alterations that are fundamentally different from myocyte hypertrophy [6, 13]. Concordantly, the classification profiles of MEF2 target genes identified in the present study, revealed surprisingly little overlap with those observed with massive hypertrophic remodeling in early pressure overload (http://cardiogenomics.med.harvard.edu). In contrast, our gene profiles correlate well with those observed in gene chip analysis of human end-stage idiopathic dilated cardiomyopathy [27] and with the most characteristic pathological features of human end-stage dilated cardiomyopathy, which include myocyte lengthening (elongation), myofibril degeneration, a dynamic redistribution of cytoskeletal structures, alterations in mitochondria number and morphology (energy metabolism), and extensive fibrosis [7, 8].

One of the striking observations in the present study included the elongated morphology of cardiomyocytes and the sequential disassembly of myofibril components upon increasing MEF2 transcriptional activity, which affected both M-band and Z-disc components. Many cardiomyopathic conditions share the common characteristic of myofibril degeneration, which contrasts the promotion of sarcomere organization during early phases of cardiac hypertrophy. Loss of myofibrils is the most obvious structural change in dilated cardiomyopathy [28] and sarcomeric disarray is characteristic of end-staged failing human hearts [8]. Features of human dilated cardiomyopathy include increased myocardial mass and biventricular chamber dilation, myocyte and myofibril disarray, and loss of contractile material [7].

Another striking observation was the redistribution of focal adhesions sites that accompanied elongated cardiomyocytes upon MEF2 activation. Cardiomyocytes from MLP knockout mice and tropomodulin-overexpressing transgenic mice [29], two models with severe chamber dilation, present striking alterations of their cell-matrix as well as their cell-cell contacts. Isolated myocytes from these cardiomyopathic models elicit a more irregular shape compared with their wild-type counterparts [30], which may serve to increase the number of focal contacts between neighboring cells. Specifically, the costameric protein vinculin showed patchy staining near the plasma membranes in MLP null cardiomyocytes compared with the regular well-ordered striations that are observed at the membrane of wildtype cardiomyocytes [30]. These differences in vinculin subcellular distribution mimic the changes observed in our study on vinculin

localization in hypertrophic and elongated myocytes following MEF2 activation. Increased expression of extracellular matrix components, as found in our gene profiles, and a general upregulation of vinculin was described in patients with DCM [8, 31], suggesting that this phenomenon might not be restricted to mouse models for this disease.

In this study, microarray analysis provided mechanistic insights into the cardiomyopathic remodeling processes, as many of the genes activated by MEF2 are involved in cytoskeletal remodeling and focal adhesion assembly. We further demonstrated that one of these genes, DMPK, is a direct target of MEF2. More importantly, knockdown of DMPK expression sufficiently inhibited cardiomyocyte elongation and sarcomere disassembly in response to elevated MEF2 activity. Myotonic dystrophy 1 is associated with expansion of untranslated CTG repeats in the 3 prime UTR of *dmpk*, which is believed to result in a pathological accumulation of RNA in the nucleus [23, 32]. In the heart, however, the DM1 cardiac pathology may be more directly due to increased DMPK expression, rather than RNA toxicity [33]. Indeed, transgenic mice overexpressing DMPK display a heart failure phenotype, with extensive myocyte disarray and interstitial fibrosis [25].

Findings in several other studies underline the potential role of DMPK in myocyte remodeling. The *dmpk* gene encodes a protein kinase related to the Rho family of protein kinases, which are associated with actin cytoskeletal remodeling [34-37]. DMPK shares a high homology with myotonic dystrophy kinase-related Cdc42 binding kinases (MRCKs) [34]. MRCK and Cdc42 colocalize at the cell periphery inducing actin and myosin reorganization and focal adhesion complex formation [38]. Cdc42 has been described to play a critical role in sarcomere assembly and elongation of cardiomyocytes [39]. DMPK is also known to interact with Rac-1 [40], and both DMPK and Rac-1 are able to phosphorylate and inhibit myosin phosphatase [41]. Inhibition of myosin phosphatase and associated increase in myosin phosphorylation leads to an increase in stress fibers and focal adhesion sites and is important for sarcomere organization [37, 42]. Expression of constitutively activated Rac1 in the heart induces focal adhesion redistribution and cardiac dilation [43]. We observed localization of focal adhesion complexes to the most distal ends of elongated cardiomyocytes upon MEF2 activation. Interestingly, overexpression of human DMPK in yeast resulted in polarized elongated cell growth [44]. Furthermore, during differentiation of human skeletal muscle cells DMPK localizes towards the terminal parts of elongating cells [45].

In conclusion, our findings identify DMPK as a direct transcriptional target of MEF2, promoting myocyte elongation, myofibril degeneration and polarized focal adhesion redistribution, changes of the heart muscle, which are characteristic of dilated cardiomyopathy.

ACKNOWLEDGEMENTS

The authors would like to thank Marc van de Wetering and Hans Clevers for reagents and advice with the generation of stable cell lines. This work was supported by grants 902-16-275, 912-04-054 and 912-04-017 from the Netherlands Organization for Health Research and Development (ZonMW), grant 2003B258 of the Netherlands Heart Foundation, and by the European Union Contract No. LSHM-CT-2005-018833/EUGeneHeart (to L.J.D.W.).

REFERENCES

1. Gossett L.A., Kelvin D.J., Sternberg E.A., Olson E.N. A new myocyte-specific enhancer-binding factor that recognizes a conserved element associated with multiple muscle-specific genes. Mol Cell Biol 1989;9(11):5022-33.
2. Black B.L., Olson E.N. Transcriptional control of muscle development by myocyte enhancer factor-2 (MEF2) proteins. Annu Rev Cell Dev Biol 1998;14:167-96.
3. McKinsey T.A., Zhang C.L., Olson E.N. MEF2: a calcium-dependent regulator of cell division, differentiation and death. Trends Biochem Sci 2002;27:40-47.
4. Olson E.N., Perry M., Schulz R.A. Regulation of muscle differentiation by the MEF2 family of MADS box transcription factors. Dev Biol 1995;172(1):2-14.
5. Frey N., Katus H.A., Olson E.N., Hill J.A. Hypertrophy of the heart: a new therapeutic target? Circulation 2004;109(13):1580-9.
6. van Oort R.J., van Rooij E., Bourajjaj M., Schimmel J., Jansen M.A., van der Nagel R., Doevendans P.A., Schneider M.D., van Echteld C.J., De Windt L.J. MEF2 activates a genetic program promoting chamber dilation and contractile dysfunction in calcineurin-induced heart failure. Circulation 2006;114(4):298-308.
7. Beltrami C.A., Finato N., Rocco M., Feruglio G.A., Puricelli C., Cigola E., Sonnenblick E.H., Olivetti G., Anversa P. The cellular basis of dilated cardiomyopathy in humans. J Mol Cell Cardiol 1995;27(1):291-305.
8. Schaper J., Froede R., Hein S., Buck A., Hashizume H., Speiser B., Friedl A., Bleese N. Impairment of the myocardial ultrastructure and changes of the cytoskeleton in dilated cardiomyopathy. Circulation 1991;83(2):504-14.
9. Passier R., Zeng H., Frey N., Naya F.J., Nicol R.L., McKinsey T.A., Overbeek P., Richardson J.A., Grant S.R., Olson E.N. CaM kinase signaling induces cardiac hypertrophy and activates the MEF2 transcription factor in vivo. J Clin Invest 2000;105(10):1395-406.
10. Naya F.J., Black B.L., Wu H., Bassel-Duby R., Richardson J.A., Hill J.A., Olson E.N. Mitochondrial deficiency and cardiac sudden death in mice lacking the MEF2A transcription factor. Nat Med 2002;8(11):1303-9.
11. Lu J., McKinsey T.A., Nicol R.L., Olson E.N. Signal-dependent activation of the MEF2 transcription factor by dissociation from histone deacetylases. Proc Natl Acad Sci U S A 2000;97(8):4070-5.
12. Nadruz W., Jr., Kobarg C.B., Constancio S.S., Corat P.D., Franchini K.G. Load-induced transcriptional activation of c-jun in rat myocardium: regulation by myocyte enhancer factor 2. Circ Res 2003;92(2):243-51.
13. Xu J., Gong N.L., Bodi I., Aronow B.J., Backx P.H., Molkentin J.D. Myocyte enhancer factors 2A and 2C induce dilated cardiomyopathy in transgenic mice. J Biol Chem 2006;281(14):9152-62.

14. He T.C., Zhou S., da Costa L.T., Yu J., Kinzler K.W., Vogelstein B. A simplified system for generating recombinant adenoviruses. Proc Natl Acad Sci U S A 1998;95(5):2509-14.
15. Taigen T., De Windt L.J., Lim H.W., Molkentin J.D. Targeted inhibition of calcineurin prevents agonist-induced cardiomyocyte hypertrophy. Proc Natl Acad Sci U S A 2000;97(3):1196-201.
16. Rybkin, II, Markham D.W., Yan Z., Bassel-Duby R., Williams R.S., Olson E.N. Conditional expression of SV40 T-antigen in mouse cardiomyocytes facilitates an inducible switch from proliferation to differentiation. J Biol Chem 2003;278(18):15927-34.
17. Ehler E., Rothen B.M., Hammerle S.P., Komiyama M., Perriard J.C. Myofibrillogenesis in the developing chicken heart: assembly of Z-disk, M-line and the thick filaments. J Cell Sci 1999;112 (Pt 10):1529-39.
18. Obermann W.M., Gautel M., Steiner F., van der Ven P.F., Weber K., Furst D.O. The structure of the sarcomeric M band: localization of defined domains of myomesin, M-protein, and the 250-kD carboxy-terminal region of titin by immunoelectron microscopy. J Cell Biol 1996;134(6):1441-53.
19. Agarkova I., Schoenauer R., Ehler E., Carlsson L., Carlsson E., Thornell L.E., Perriard J.C. The molecular composition of the sarcomeric M-band correlates with muscle fiber type. Eur J Cell Biol 2004;83(5):193-204.
20. Czubryt M.P., McAnally J., Fishman G.I., Olson E.N. Regulation of peroxisome proliferator-activated receptor gamma coactivator 1 alpha (PGC-1 alpha) and mitochondrial function by MEF2 and HDAC5. Proc Natl Acad Sci U S A 2003;100(4):1711-6.
21. Brook J.D., McCurrach M.E., Harley H.G., Buckler A.J., Church D., Aburatani H., Hunter K., Stanton V.P., Thirion J.P., Hudson T., et al. Molecular basis of myotonic dystrophy: expansion of a trinucleotide (CTG) repeat at the 3' end of a transcript encoding a protein kinase family member. Cell 1992;68(4):799-808.
22. Tsilfidis C., MacKenzie A.E., Mettler G., Barcelo J., Korneluk R.G. Correlation between CTG trinucleotide repeat length and frequency of severe congenital myotonic dystrophy. Nat Genet 1992;1(3):192-5.
23. Mahadevan M., Tsilfidis C., Sabourin L., Shutler G., Amemiya C., Jansen G., Neville C., Narang M., Barcelo J., O'Hoy K., et al. Myotonic dystrophy mutation: an unstable CTG repeat in the 3' untranslated region of the gene. Science 1992;255(5049):1253-5.
24. Fu Y.H., Pizzuti A., Fenwick R.G., Jr., King J., Rajnarayan S., Dunne P.W., Dubel J., Nasser G.A., Ashizawa T., de Jong P., et al. An unstable triplet repeat in a gene related to myotonic muscular dystrophy. Science 1992;255(5049):1256-8.
25. O'Cochlain D.F., Perez-Terzic C., Reyes S., Kane G.C., Behfar A., Hodgson D.M., Strommen J.A., Liu X.K., van den Broek W., Wansink D.G., Wieringa B., Terzic A. Transgenic overexpression of human DMPK accumulates into hypertrophic cardiomyopathy, myotonic myopathy and hypotension traits of myotonic dystrophy. Hum Mol Genet 2004;13(20):2505-18.
26. Hoshijima M., Chien K.R. Mixed signals in heart failure: cancer rules. J Clin Invest 2002;109(7):849-55.
27. Grzeskowiak R., Witt H., Drungowski M., Thermann R., Hennig S., Perrot A., Osterziel K.J., Klingbiel D., Scheid S., Spang R., Lehrach H., Ruiz P. Expression profiling of human idiopathic dilated cardiomyopathy. Cardiovasc Res 2003;59(2):400-11.
28. Mann D.L., Urabe Y., Kent R.L., Vinciguerra S., Cooper G.t. Cellular versus myocardial basis for the contractile dysfunction of hypertrophied myocardium. Circ Res 1991;68(2):402-15.

29. Sussman M.A., Welch S., Cambon N., Klevitsky R., Hewett T.E., Price R., Witt S.A., Kimball T.R. Myofibril degeneration caused by tropomodulin overexpression leads to dilated cardiomyopathy in juvenile mice. J Clin Invest 1998;101(1):51-61.
30. Ehler E., Horowits R., Zuppinger C., Price R.L., Perriard E., Leu M., Caroni P., Sussman M., Eppenberger H.M., Perriard J.C. Alterations at the intercalated disk associated with the absence of muscle LIM protein. J Cell Biol 2001;153(4):763-72.
31. Wilke A., Schonian U., Herzum M., Hengstenberg C., Hufnagel G., Brilla C.G., Maisch B. [The extracellular matrix and cytoskeleton of the myocardium in cardiac inflammatory reaction]. Herz 1995;20(2):95-108.
32. Davis B.M., McCurrach M.E., Taneja K.L., Singer R.H., Housman D.E. Expansion of a CUG trinucleotide repeat in the 3' untranslated region of myotonic dystrophy protein kinase transcripts results in nuclear retention of transcripts. Proc Natl Acad Sci U S A 1997;94(14):7388-93.
33. Mahadevan M.S., Yadava R.S., Yu Q., Balijepalli S., Frenzel-McCardell C.D., Bourne T.D., Phillips L.H. Reversible model of RNA toxicity and cardiac conduction defects in myotonic dystrophy. Nat Genet 2006;38(9):1066-70.
34. Wansink D.G., van Herpen R.E., Coerwinkel-Driessen M.M., Groenen P.J., Hemmings B.A., Wieringa B. Alternative splicing controls myotonic dystrophy protein kinase structure, enzymatic activity, and subcellular localization. Mol Cell Biol 2003;23(16):5489-501.
35. Amano M., Chihara K., Nakamura N., Kaneko T., Matsuura Y., Kaibuchi K. The COOH terminus of Rho-kinase negatively regulates rho-kinase activity. J Biol Chem 1999;274(45):32418-24.
36. Amano M., Fukata Y., Kaibuchi K. Regulation and functions of Rho-associated kinase. Exp Cell Res 2000;261(1):44-51.
37. Kaibuchi K., Kuroda S., Amano M. Regulation of the cytoskeleton and cell adhesion by the Rho family GTPases in mammalian cells. Annu Rev Biochem 1999;68:459-86.
38. Leung T., Chen X.Q., Tan I., Manser E., Lim L. Myotonic dystrophy kinase-related Cdc42-binding kinase acts as a Cdc42 effector in promoting cytoskeletal reorganization. Mol Cell Biol 1998;18(1):130-40.
39. Nagai T., Tanaka-Ishikawa M., Aikawa R., Ishihara H., Zhu W., Yazaki Y., Nagai R., Komuro I. Cdc42 plays a critical role in assembly of sarcomere units in series of cardiac myocytes. Biochem Biophys Res Commun 2003;305(4):806-10.
40. Shimizu M., Wang W., Walch E.T., Dunne P.W., Epstein H.F. Rac-1 and Raf-1 kinases, components of distinct signaling pathways, activate myotonic dystrophy protein kinase. FEBS Lett 2000;475(3):273-7.
41. Muranyi A., Zhang R., Liu F., Hirano K., Ito M., Epstein H.F., Hartshorne D.J. Myotonic dystrophy protein kinase phosphorylates the myosin phosphatase targeting subunit and inhibits myosin phosphatase activity. FEBS Lett 2001;493(2-3):80-4.
42. Aoki H., Sadoshima J., Izumo S. Myosin light chain kinase mediates sarcomere organization during cardiac hypertrophy in vitro. Nat Med 2000;6(2):183-8.
43. Sussman M.A., Welch S., Walker A., Klevitsky R., Hewett T.E., Price R.L., Schaefer E., Yager K. Altered focal adhesion regulation correlates with cardiomyopathy in mice expressing constitutively active rac1. J Clin Invest 2000;105(7):875-86.
44. Sasagawa N., Kino Y., Takeshita Y., Oma Y., Ishiura S. Overexpression of human myotonic dystrophy protein kinase in Schizosaccharomyces pombe induces an abnormal polarized and swollen cell morphology. J Biochem (Tokyo) 2003;134(4):537-42.
45. Beffy P., Barsanti C., Del Carratore R., Simi S., Benedetti P.A., Benzi L., Prelle A., Ciscato P., Simili M. Expression and localization of myotonic dystrophy protein kinase in human skeletal muscle cells determined with a novel antibody: possible role of the protein in cytoskeleton rearrangements during differentiation. Cell Biol Int 2005;29(9):742-53.